Available online at www.sciencedirect.com
ScienceDirect
Nuclear Physics B Proceedings Supplement 00 (2014) 1–6
Nuclear Physics B Proceedings Supplement

Angular analysis and differential branching fraction of the decay: $B \to K^* \mu^+ \mu^-$.

K. Mazumdar for CMS Collaboration

Tata Institute of Fundamnetal Research, Mumbai, India.

Abstract

Measurements of rare B meson decay properties provide an alternative approach to direct searches for physics beyond the Standard Model. These decays, which proceed through flavor-changing neutral currents, can have interferences from new physics through loop diagrams and hence an excellent probe. In particular, the angular distribution of the decay $B \to K^* \mu^+ \mu^-$ can be measured to estimate the forward-backward asymmetries of the muons, the longitudinal polarization fractions of K^* and the differential branching fractions, as a function of the dimuon invariant mass. Results based on data recorded by the CMS experiment at centre-of-mass energy of 7 TeV are presented.

Keywords: FCNC decays, $B \to K^* \mu^+ \mu^-$, CMS

1. Introduction

Flavour changing neutral currents (FCNC) are forbidden in standard model (SM) at tree level. They can appear in higher order quantum processes involving loops and boxes and hence have very small rates. However, new and heavy particles invoked in theories beyond SM, and, which cannot be produced directly in experiments, can appear virtually in such diagrams. Thus non-SM physics is capable of modifying the predictions of SM in a subtle way. The effective Hamiltonian for such transitions can be expressed in terms of linear combinations of products of higher dimensional operators and the Wilson coefficients, though several of these coefficients are strongly constrained by experiments. Importantly, detailed angular analyses lead to the separation of the Wilson coefficients. Currently, study of FCNC processes is even more pertinent, since no direct evidence of new physics beyond SM has been found till now.

The decay $B^0 \to K^{*0} \ell^+ \ell^-$ (and its charge conjugate) proceeds, at leading order, via electroweak penguin and box diagrams as shown in Fig. 1. Various angular observables for the decay are predicted quite accurately in SM; in particular, the uncertainties for relevant form factors in dilepton invariant mass ($m_{\ell\ell}$) region away from the J/ψ and $\psi' \equiv \psi(2S)$ resonances are under good control. At low recoil of the K^{*0}, $q^2 = m^2_{\ell\ell}$, the electromagnetic operator is enhanced for $B^0 \to K^{*0} \ell^+ \ell^-$ decay as opposed to $B^0 \to K^0 \ell^+ \ell^-$. On the other hand, the semileptonic decay involving the vector and axial vector currents are important at high q^2. Thus an angular analysis, as a function of q^2, is an interesting probe to possible new physics affecting the final states. Additionally, the forward-backward asymmetry of the leptons is also senstive to the phases of the Wilson coefficients. Hence experimental pursuits are very relevant and measurements can be compared with theoretical predictions from SM [1, 2, 3].

Experimentally, presence of dimuons in the final state makes the measurement relatively free of background compared to electrons. Further, the availability of control channels, $B^0 \to K^{*0} J/\psi(\to$

$\mu^+\mu^-$) and $B^0 \to K^{*0}\psi(2S)(\to \mu^+\mu^-)$, makes the experimental analyses relatively easy. However, the pre-LHC studies suffer from large statistical uncertainties [4, 5, 6]. With LHC data, measurements of the forward-backward asymmetry of the muons, A_{FB}, the fraction of longitudinal polarization of the K^{*0}, F_L, and the differential branching fraction, $d\mathcal{B}/dq^2$, as a function of q^2 have been performed [7, 8]. Studies done by CMS collaboration using pp collision data collected at centre-of-mass energy of 7 TeV, corresponding to an integrated luminosity of 5.2 ± 0.1 fb^{-1}, is reported here.

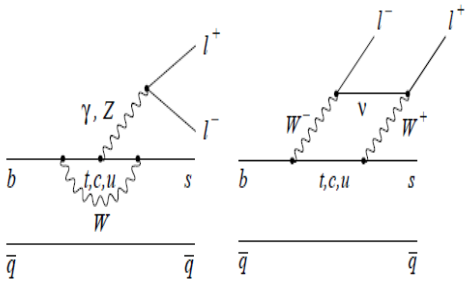

Figure 1: Dominant Standard Model Feynman diagrams for the decay $\overline{B}^0 \to \overline{K}^{*0}\mu^+\mu^-$.

2. Experimental Measurements

2.1. Methodology

Experimentally the decay of $K^{*0}(892\ \mathrm{GeV}/c^2)$ is reconstructed through its decay into $K^+\pi^-$. If the charge assignment for the hadron tracks is ambiguous, ie, the invariant masses for both $K^+\pi^-$ and $K^-\pi^+$ combinations are within 50 Mev/c^2 of the nominal mass, the event is rejected. The amount of wrong assignment is estimated to be 8% from simulation. The candidate B^0 is reconstructed by fitting two muons and two hadron track candidates to a common vertex. The signal sample is complementary to the normalization/control sample due to the demarcation: $m_{J/\psi} - 5\sigma_{m(\mu\mu)} < m(\mu\mu) < m_{J/\psi} + 3\sigma_{m(\mu\mu)}$ and $|m(\mu\mu) - M_{\psi(2S)}| < 3\sigma_{m(\mu\mu)}$; the asymmetric cut accounts for the radiative tail of the dimuon spectrum from J/ψ resonance. $\psi(2S)$ has much smaller signal.

The parameters of interest, A_{FB} and F_L are determined from unbinned extended maximum-likelihood fits in bins of q^2 as a function of the invariant mass of the $K^+\pi^-\mu^+\mu^-$ system and two angular variables, as shown through a cartoon in Fig. 2. The angle θ_K is defined as the angle between the kaon momentum and the opposite direction of the B^0 ($\overline{B}^0$) in the K^{*0} ($\overline{K^{*0}}$) rest frame, while the angle θ_l is defined as the angle between the positive (negative) charged muon momentum and the opposite direction of the B^0 ($\overline{B}^0$) in the dimuon reference frame. If the $K-\pi$ system is due to the decay

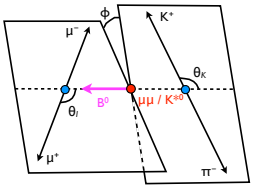

Figure 2: Definition of the angular observables for the decay $B \to K^*\mu^+\mu^-$

.

of the vector meson K^{*0} their angular distribution in the final state can be described with a P-wave, while if it is not so the description will be through a spinless S-wave. The decay rates account for both possibilities, though the S-wave fraction, given by F_S, is small with respect to the P one. Thus the differential branching fraction, also containing an interference term A_s, is described as:

$$\frac{1}{\Gamma}\frac{d^3\Gamma}{d\cos\theta_K d\cos\theta_l dq^2} = \frac{9}{16}\left\{\left[\frac{2}{3}F_S + \frac{4}{3}A_S\cos\theta_K\right](1-\cos^2\theta_l)\right.$$
$$+ (1-F_S)\left[2F_L\cos^2\theta_K(1-\cos^2\theta_l)\right.$$
$$+ \frac{1}{2}(1-F_L)(1-\cos^2\theta_K)(1+\cos^2\theta_l)$$
$$\left.\left. + \frac{4}{3}A_{FB}(1-\cos^2\theta_K)\cos\theta_l\right]\right\}.$$

The data are divided into 6 q^2 bins : $1-2$, $2-4.3$, $4.3-8.68$, $8.68-10.09$, $10.09-12.86$, $12.86-14.18$, $14.18-16$, $16-19$ GeV^2. Two control channels, corresponding to bin #3 and #5 covering the J/ψ and $\psi(2S)$ resonance regions, are used to validate the analysis. For each q^2 bin, the probability density function (PDF) is a function of m, $\cos\theta_K$, and $\cos\theta_l$ and has the form

$$\mathrm{PDF} = Y_S \cdot S(m) \cdot S(cos\theta_K, cos\theta_l) \cdot \epsilon(cos\theta_K, cos\theta_l)$$
$$+ Y_{Bc} \cdot B_c(m) \cdot B_c(cos\theta_K) \cdot B_c(\cos\theta_l)$$
$$+ Y_{Bp} \cdot B_p(m) \cdot B_p(cos\theta_K) \cdot B_p(\cos\theta_l)$$

where Y_S, Y_{Bc}, and Y_{Bp} are the yields of the signal, "combinatorial" and "peaking" backgrounds

respectively. The combinatorial part accounts for misreconstructed B^0 from randomly associated dimuons to hadrons, and the peaking part to the feed-through from the control channels; The product $S(m)\cdot S(cos\theta_K, cos\theta_l)$ describes the signal shape given in terms of invariant mass variable and the theoretical signal shape in terms of the angular variables. $S(m)$ is a sum of 2 Gaussians with a common mean. The efficiency function $\epsilon(cos\theta_K, cos\theta_l)$ takes into account the possibility of mistagging B^0 as $\overline{B^0}$ (and vice versa) and is obtained from a polynomial fit to 2d histograms for efficiency in terms of 5 $cos\theta_l$ and 6 $cos\theta_K$ bins.

The differential branching fraction for the decay $B^0 \to K^{*0}\mu^+\mu^-$, given by $d\mathcal{B}/dq^2$, is measured, using the results of A_{FB} and F_L, and from an unbinned maximum likelihood fit, in terms of the branching fraction for normalization channel $B^0 \to K^{*0}J/\psi$:

$$\frac{d\mathcal{B}(B^0 \to K^{*0}\mu^+\mu^-)}{dq^2} = \frac{Y_S}{Y_N}\frac{\epsilon_N}{\epsilon_S}\frac{\mathcal{B}(B^0 \to K^{*0}J/\psi)}{dq^2},$$

where Y_S, Y_N are the event yields and ϵ_S, ϵ_N are the efficiencies of the signal and the normalization channels respectively. Several methods are used to validate the formalism of the fit. Discrepancies in the control channel compared to theoretical predictions are treated as systematic uncertainties.

2.2. Systematic uncertainty

Various sources of systmatic uncertainties for the measurement of A_{FB}, F_L has been considered and summarized in Table 1. For the branching ratio measurement, $d\mathcal{B}/dq^2$, the systematic uncertainty is pretty large adding upto above 20%. An additional normalization systematic uncertainty of 4.6% arises due to the uncertainty on the branching fraction of the normalization mode.

3. Results

Figures 3 – 6 display the $K^+\pi^-\mu^+\mu^-$ invariant mass distribution for different signal q^2 bins. Overlaid on each mass distribution is the projection of the unbinned maximum likelihood fit. The blue, red and magenta lines represent the signal, the combinatorial and the peaking background components of the PDF respectively. The last component is present only for the q^2 bins relevant for J/ψ and $\psi(2S)$ as in Fig. 6. Figure 4 corresponds to the validation channel due to $B^0 \to K^+\pi^-J/\psi$ conatining 47 000 signal events. Projections as a function of variables $cos\theta_l$ and $cos\theta_K$ are presented in Fig.s 7 and 8 respectively. The measured values for this channel are $F_L = 0.554 \pm 0.004(\text{stat.})$ and $A_FB = -0.004 \pm 0.004(\text{stat.})$, compatible with expectation for no asymmetry. The other 2 parameters do not depend on q^2 and are detrmined to be $F_S = 0.01 \pm 0.01(\text{stat.})$ and $A_S = -0.10 \pm 0.01(\text{stat.})$.

Table 1: Uncorrelated systematic uncertainty contributions for the measurements of F_L,A_{FB}.

Systematic uncertainty	F_L	A_{FB}
Efficiency statistical uncertainty	0.005 – 0.007	0.003 – 0.005
Fit algorithm bias (toy MC)	0.003 – 0.040	0.012 – 0.077
Fit ingredients bias (full MC)	0	0 – 0.017
Incorrect CP assignment of decay	0.002 – 0.006	0.002 – 0.006
Effect of $K\pi$ S-wave contribution	0.005 – 0.023	0.006 – 0.014
Peaking background mass shape	0 – 0.026	0 – 0.008
Combinatorial background shapes vs $\cos\theta_{\ell,K}$	0.003 – 0.179	0.004 – 0.161
Angular resolution	0 – 0.019	0
Signal mass shape	0	0
Efficiency shape	0.016	0.004
Total systematic uncertainty	0.031 – 0.186	0.018 – 0.179

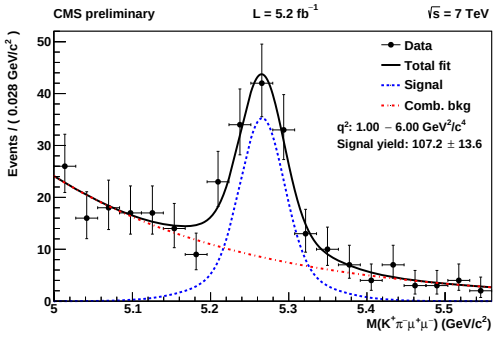

Figure 3: Distribution of invariant mass of $K^\pm\pi^\mp\mu^+\mu^-$ system in data and fit alongwith signal and background components for $1 < q^2 < 6$ GeV/c^2

.

The F_L and A_{FB} measurements presented in a two-dimensional space, as shown in Fig. 9, imply that all measurements lie within the physically-allowed domain.

Figures 10 – 12 present, the measurements of CMS compared with other experiments where, for each q^2 bin, all data points but for CMS and LHCb,

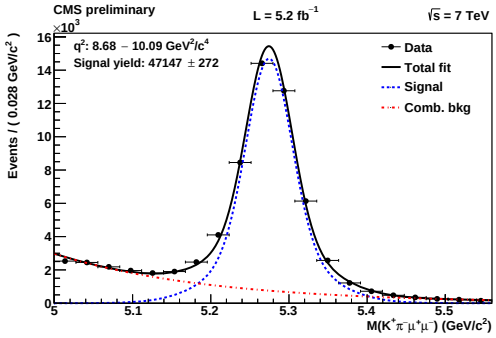

Figure 4: Distribution of invariant mass of $K^{\pm}\pi^{\mp}\mu^{+}\mu^{-}$ system in data and fit alongwith signal and background components for $8.68 < q^2 < 10.09$ GeV/c^2

.

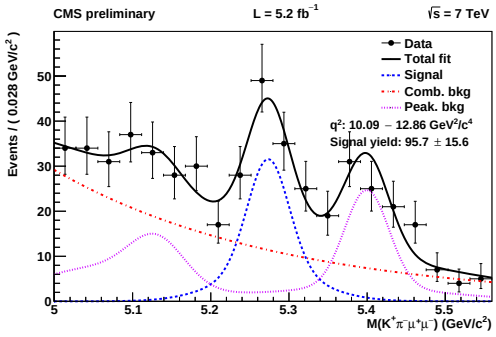

Figure 5: Distribution of invariant mass of $K^{\pm}\pi^{\mp}\mu^{+}\mu^{-}$ system in data and fit alongwith signal and background components for $10.09 < q^2 < 12.86$ GeV/c^2

.

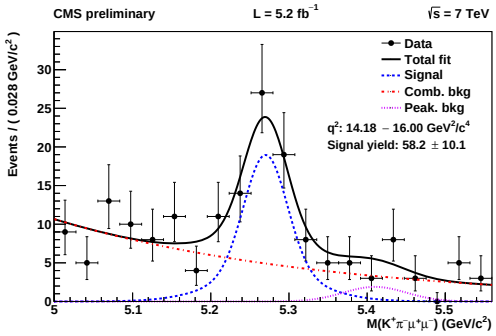

Figure 6: Distribution of invariant mass of $K^{\pm}\pi^{\mp}\mu^{+}\mu^{-}$ system in data and fit alongwith signal and background components for $14.18 < q^2 < 16.00$ GeV/c^2

.

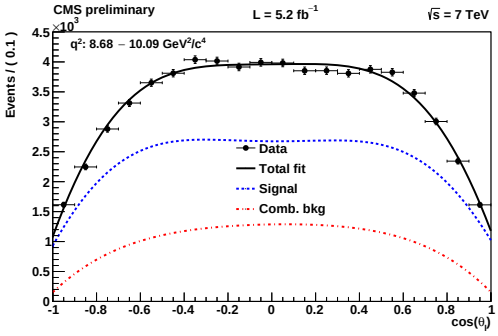

Figure 7: Distribution of $cos\theta_l$ in data and fit alongwith signal and background components for validation channel $8.68 < q^2 < 10.09$ GeV/c^2

.

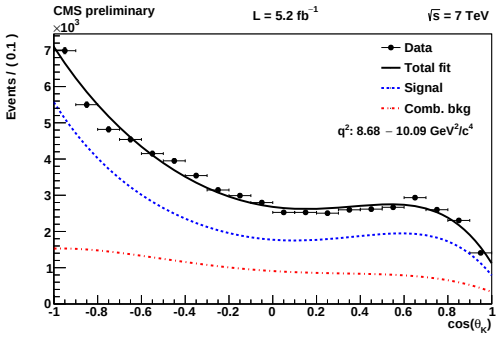

Figure 8: Distribution of $cos\theta_K$ in data and fit alongwith signal and background components for $8.68 < q^2 < 10.09$ GeV/c^2

.

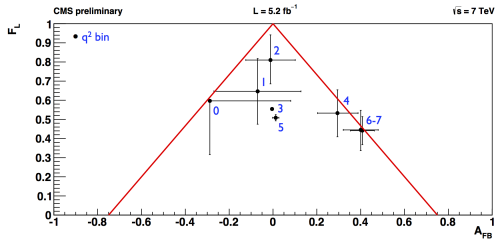

Figure 9: K^{*0} longitudinal polarization fraction versus forward-backward asymmetry of the muons (errors are purely statistical)

.

are slightly shifted along the x-axis for ease in readability. The gray regions correspond to the J/ψ and $\psi(2S)$ resonances. The prediction from SM is given by the blue (dark) regions where it was rate-averaged across the bins to allow direct comparison to the data points.

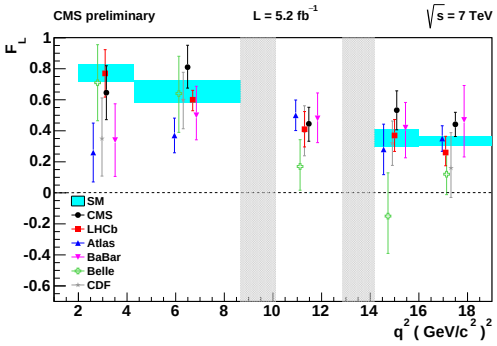

Figure 10: K^{*0} longitudinal polarization as a function of q^2 measured in different experiments, compared with standard model prediction averaged over a given q^2 range.

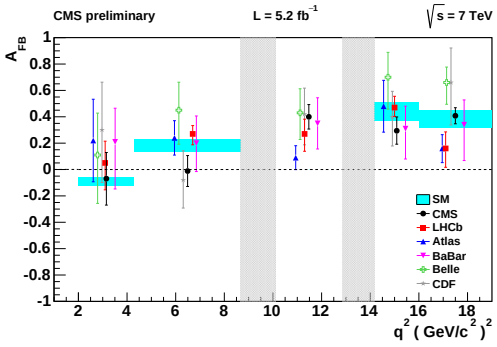

Figure 11: Muon forward-backward asymmetry as a function of q^2 measured in different experiments, compared with standard model prediction averaged over a given q^2 range.

4. Conclusion

The angular analaysis of $B^0 \to K^{*0}\mu^+\mu^-$ decay, performed in CMS experiment, using data collected at centre-of-mass energy of 7 TeV has been presented. Unbinned maximum likelihood fits were performed in bins of the dimuon invariant mass squared (q^2) with three independent variables: $K^+\pi^-\mu^+\mu^-$ invariant mass, $\cos\theta_K$, and $\cos\theta_l$ to obtain values of A_{FB}, and F_L. Using these results, unbinned maximum likelihood fits to the

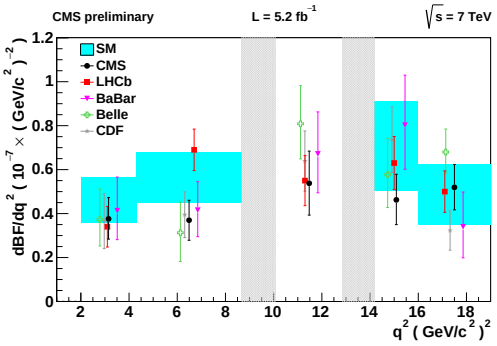

Figure 12: Branching fraction as a function of q^2 measured in different experiments, compared with standard model prediction averaged over a given q^2 range.

$K^+\pi^-\mu^+\mu^-$ invariant mass in various q^2 bins were used to extract $d\mathcal{B}/dq^2$. No deviations from the standard model predictions are found. With data collected at 8 TeV, corresponding to much more event statistics, the branching fraction will be measured more accurately. Further it will also be possible to measure the zero crossing point of A_{FB} and other angular variables.

References

[1] F. Kruger, L. M. Sehgal, N. Sinha, R. Sinha; Angular distribution and CP asymmetries in the decays $\bar{B} \to K^-\pi^+e^-e^+$ and $\bar{B} \to \pi^-\pi^+e^-e^+$.
doi: 10.1103/PhysRevD.61.114028

[2] C. Bobeth, G. Hiller, D. van Dyk; The Benefits of $\bar{B} \to \bar{K}^{(*)}\ell^+\ell^-$ Decays at Low Recoil.
doi: 10.1007/JHEP07(2010)098

[3] C. Bobeth, G. Hiller, D. van Dyk; The decay $\bar{B} \to \bar{K}^*\ell^+\ell^-$ at low hadronic recoil and model-independent $\Delta B = 1$ constraints.
doi: 10.1007/JHEP01(2012)107

[4] BaBar Collaboration; Angular distributions in the decay $B \to K^*l^+l^-$.
doi: 10.1103/PhysRevD.79.031102

[5] Belle Collaboration; Measurement of the Differential Branching Fraction and Forward-Backword Asymmetry for $B \to K^*l^+l^-$.
doi: 10.1103/PhysRevLett.103.171801

[6] CDF Collaboration; Measurements of the Angular Distributions in the Decays $B \to K^*\mu^+\mu^-$ at CDF.
doi: 10.1103/PhysRevLett.108.081807

[7] LHCb Collaboration; Differential branching fraction and angular analysis of the decay $B^0 \to K^{*0}\mu^+\mu^-$.
doi: 10.1103/PhysRevLett.108.181806

[8] CMS Collaboration; Angular analysis and branching fraction measurement of the decay $B \to K^*\mu^+\mu^-$.
doi: 10.1016/j.physletb.2013.10.017